Improved characterization of trastuzumab deruxtecan with PTCR and internal fragments implemented in middle-down MS workflows

Corentin Beaumal, Evolène Deslignière, Hélène Diemer, Christine Carapito, Sarah Cianférani, Oscar Hernandez-Alba

Analytical and Bioanalytical Chemistry
https://doi.org/10.1007/s00216-023-05059-x

RESEARCH PAPER

Improved characterization of trastuzumab deruxtecan with PTCR and internal fragments implemented in middle-down MS workflows

Corentin Beaumal[1,2] · Evolène Deslignière[1,2] · Hélène Diemer[1,2] · Christine Carapito[1,2] · Sarah Cianférani[1,2] · Oscar Hernandez-Alba[1,2]

Received: 12 September 2023 / Revised: 13 November 2023 / Accepted: 14 November 2023

Abstract

Antibody-drug conjugates (ADCs) are highly complex proteins mainly due to the structural microvariability of the mAb, along with the additional heterogeneity afforded by the bioconjugation process. Top-down (TD) and middle-down (MD) strategies allow the straightforward fragmentation of proteins to elucidate the conjugated amino acid residues. Nevertheless, these spectra are very crowded with multiple overlapping and unassigned ion fragments. Here we report on the use of dedicated software (ClipsMS) and application of proton transfer charge reduction (PTCR), to respectively expand the fragment ion search space to internal fragments and improve the separation of overlapping fragment ions for a more comprehensive characterization of a recently approved ADC, trastuzumab deruxtecan (T-DXd). Subunit fragmentation allowed between 70 and 90% of sequence coverage to be obtained. Upon addition of internal fragment assignment, the three subunits were fully sequenced, although internal fragments did not contribute significantly to the localization of the payloads. Finally, the use of PTCR after subunit fragmentation provided a moderate sequence coverage increase between 2 and 13%. The reaction efficiently decluttered the fragmentation spectra allowing increasing the number of fragment ions characteristic of the conjugation site by 1.5- to 2.5-fold. Altogether, these results show the interest in the implementation of internal fragment ion searches and more particularly the use of PTCR reactions to increase the number of signature ions to elucidate the conjugation sites and enhance the overall sequence coverage of ADCs, making this approach particularly appealing for its implementation in R&D laboratories.

Keywords Trastuzumab deruxtecan · Middle-down (MD) · Electron transfer dissociation (ETD) · Proton transfer charge reduction (PTCR) · Internal fragments

Abbreviations

ADC	Antibody-drug conjugate
AGC	Automatic gain control
avDAR	Average drug-to-antibody ratio
CID	Collision-induced dissociation
ETD	Electron transfer dissociation
EThcD	Electron transfer/higher-energy collision dissociation
Fc/2	Half crystallizable fragment
HCD	Higher-energy collision dissociation
Hc	Heavy chain
Lc	Light chain
LC	Liquid chromatography
mAb	Monoclonal antibody
MS	Mass spectrometry
nMS	Native mass spectrometry
PTCR	Proton transfer charge reduction
PTM	Post-translational modification
RPLC	Reverse-phase liquid chromatography
SEC	Size exclusion chromatography
T-DXd	Trastuzumab deruxtecan
TFA	Trifluoroacetic acid
TD/MD-MS	Top-down/middle-down mass spectrometry

✉ Oscar Hernandez-Alba
ahernandez@unistra.fr

[1] Laboratoire de Spectrométrie de Masse Bio Organique, IPHC UMR 7178, CNRS, Université de Strasbourg, 67087 Strasbourg, France

[2] Infrastructure Nationale de Protéomique ProFI - FR2048, Strasbourg, France

Published online: 27 November 2023

Introduction

From the first approval until today, monoclonal antibodies (mAbs) have experienced a continuous evolution that has changed the treatment of an array of diseases. This kind of therapeutics has proven its efficiency not only in oncology but also in immune-mediated disorders, infectious diseases, and cardiovascular disorders, among others, showcasing the therapeutic versatility of these proteins [1]. Currently, more than 170 mAbs are approved or under review by regulatory agencies, and more than 1200 mAbs are estimated to be in clinical trials [2]. Concomitantly, this outstanding evolution has motivated the development of other mAb-related therapeutic proteins, among which antibody-drug conjugates (ADCs)—constituted of a mAb, a linker, and a payload—are one of the most prominent formats [3, 4]. Different classes of conjugated mAbs have been reported with different bioconjugation strategies (cysteine [5], lysine [6], site [7], engineered [8], and unnatural [9] residue-specific ADCs), and different types of cargo molecules such as tubulin inhibitors, DNA damaging agents, and immunomodulators [10]. The size (around 150 kDa), the intrinsic primary sequence microvariability of mAbs (with tens of post-translational modifications, PTMs) [11], and the additional complexity arising from the bioconjugation process of different payloads make the characterization of these molecules particularly challenging.

In this context, native mass spectrometry (nMS), either as a standalone technique or in combination with liquid chromatography (LC), has significantly contributed to the characterization of ADCs of increased complexity [12–14]. However, the conjugation location afforded by these techniques is limited to the subunit level, and the combination of complementary MS-based methods is crucial to determining modified amino acid residues. Top-down and middle-down mass spectrometry (TD/MD-MS) have emerged as complementary approaches consisting of the fragmentation of the proteins at the intact level (TD-MS) or the subunit level after a limited proteolysis step (MD-MS) with several activation techniques [15], including electron-based dissociations (ExD), collision-induced dissociation (CID), electron-transfer/higher-energy dissociation (EThcD), and ultraviolet photodissociation (UVPD). This combination allows correlating the information derived from the fragmentation spectrum with the intact mass of the protein, leading to a better characterization of protein proteoforms while limiting the introduction of primary sequence artifacts during sample preparation [16]. Outstanding outcomes have been reported for an array of proteins of different sizes and complexity, providing high sequence coverages (up to 90%) while determining the position of relevant PTMs [17, 18]. Different TD/MD-MS strategies have also been applied to mAbs [19–24] and even ADCs [25–28] using different instruments and fragmentation techniques in order to provide a thorough characterization of the primary structure. Furthermore, numerous fragment ions bearing the intact scaffold of the glycoforms and payloads are detected, allowing a precise location of these modifications that might be fragmented in the bottom-up analysis [25, 28, 29].

One of the main concerns of TD/MD-MS is the extensive exploitation of the huge amount of information generated during the fragmentation of the intact proteins. Hence, several strategies have been developed to overcome this issue, including the design of experimental workflows aiming at decluttering the highly congested fragmentation spectra [30–34] or the development of tailored bioinformatics solutions [35, 36] to identify better and assign all the different fragment ions. Proton transfer charge reduction (PTCR), an ion/ion reaction developed in the 1990s by McLuckey and coworkers [37], has been designed to reduce the charge state of gas-phase ions and spread the MS signals to a broader m/z range. More particularly, the ions of interest undergo reaction with an anion (usually a perfluorinated compound) to lower the charge state of the ions while the anionic reactant is neutralized. Several applications of this reaction have been recently described to improve the identification of large proteoforms [32] (more than 30 kDa) or to enhance the sequence coverage of reference proteins [34] and histones [31] in TD-MS workflows. In the latter examples, the implementation of PTCR has been reported to reduce the spectral congestion in fragmentation spectra, improving the signal-to-noise ratio of fragment ions and thus providing between 5 and 20% of additional sequence coverage depending on the protein of interest and the activation technique used for sequencing [31, 33, 34]. Although quite promising, this technique has been reported in a limited number of studies and is scarcely implemented in the case of mAb-based therapeutic proteins. An additional way to enhance TD-MS protein sequencing is to take into account internal fragments [38, 39]. Despite the formation of internal fragments (secondary fragmentation of protein backbone) during TD/MD-MS analysis of intact proteins [40–43], depending on the protein size and fragmentation type, in most studies, only terminal fragment ions (containing either N- or C-terminal sides) are considered for TD/MD-MS data interpretation. Therefore, several bioinformatics tools have been developed to boost TD/MD-MS data interpretation by taking into account internal fragment ions [35, 36]. When applying these tools, not only drastic sequence coverage increase is observed [33, 38, 42, 43] (in some cases more than 40–50% of protein sequence coverage), but also more accurate determination of the specific position of modifications located in the

internal region of proteins [39, 44]. However, some previous publications reported on the increased risk of false positive fragment ion assignment when internal fragment ions are included. This risk is even more marked when several types of fragment ions are considered during ion searching [41], or when complex fragmentation techniques are used to induce the fragmentation of the backbone (such as UVPD [45]). For all those reasons, the use of internal fragments to enhance the characterization of the primary structure of proteins should be considered with caution to increase the reliance on fragment ion assignment [45].

Here, we report on the thorough characterization of a recently approved therapeutic site-specific ADC, trastuzumab deruxtecan (T-DXd), using a combination of intact MS approaches with cutting-edge MD-MS techniques encompassing the application of PTCR and internal fragment analysis. This ADC is composed of the humanized anti-HER2 trastuzumab antibody with a cleavable peptidyl-based linker (GGFG) and a potent topoisomerase I inhibitor payload (DXd) [46, 47]. The cysteines involved in the inter-chain disulfide bridges of the mAb are targeted by the bioconjugation strategy to produce a homogeneous average drug-to-antibody ratio (avDAR) of 8 [13, 46]. The fragmentation of the ADC subunits led to the characterization of the conjugation sites with sequence coverages ranging from 70 to 90%. Both conjugation sites and sequence coverage were significantly improved with the addition of internal fragment searching and PTCR reaction, increasing the number of conjugation-diagnostic fragment ions by 30–40%, along with the full sequence coverage of each T-DXd subunit. Altogether, our results pinpoint the synergy between intact MS analyses and cutting-edge MD-MS strategies to offer an in-depth characterization of a homogeneous ADC without extensive sample preparation.

Materials and methods

Materials

Trastuzumab deruxtecan (T-DXd) samples were provided by the Institut de Cancérologie Strasbourg Europe (ICANS, Strasbourg, France). All chromatographic solvents are LC-MS grade.

Middle-up analysis sample preparation

For middle-up level experiments, IdeS digestion was performed by incubating one unit of FabRICATOR enzyme (Genovis, Lund, Sweden) per microgram of ADC for 30 min at 37 °C. For denaturing conditions analysis, trifluoroacetic acid (TFA) was added to the digested ADC to a final concentration of 1%. The final concentration of the ADC in solution was 0.8 µg/µL.

Middle-down analysis sample preparation

For middle-down experiments, sample IdeS digestion was performed as mentioned for middle-up experiments. Disulfide bonds were subsequently reduced during 60 min at 37 °C in strong denaturing conditions (6 M guanidine hydrochloride) using DTT (Sigma) as a reducing agent (100 mM final DTT concentration). Finally, TFA was added to the solution at a final concentration of 1%. The final concentration of the ADC in solution was 0.7 µg/µL.

Bottom-up peptide mapping analysis

Sample preparation Ten micrograms of untreated T-DXd was solubilized in 0.1% RapiGest (Waters). Disulfide reduction was performed with 5 mM TCEP for 30 min at 57 °C. Ten millimolar of iodoacetamide for 40 min in the dark was added to alkylate-free thiol groups on cysteine residues and prevent the reformation of disulfide bridges. Digestion was performed by adding 5 µL of the prior prepared trypsin solution, i.e., 20 µg of trypsin (Promega) suspended in 100 µL of H_2O which corresponds to 1:50 enzyme to substrate ratio, at 37 °C for 5 h. The reaction was stopped by adding 1 µL of TFA. RapiGest was eliminated by incubation for 30 min at 37 °C and centrifugation at 13,000 g for 10 min.

LC-MS/MS analysis NanoLC-MS/MS analyses were performed on a Dionex UltiMate 3000 RSLC nanosystem (Thermo Scientific) coupled to an Orbitrap Eclipse™ Tribrid™ (Thermo Fisher Scientific) mass spectrometer. Mobile phase A contained 0.1% FA in water and mobile phase B contained 0.1% FA in 80% ACN/20% water. Peptides were loaded onto an Acclaim PepMap 100 C18 20 mm × 0.1 mm, 5-µm-diameter particles precolumn (Thermo Scientific) for 3 min at 10 µL/min and eluted on an Aurora Series C18 UHPLC (250 mm × 75 µm, 1.6-µm-diameter particles, IonOpticks) at a 300 nL/min flow rate following a linear gradient: 2.5% B at 0 min, 2.5% at 3 min, 7.5% at 6 min, 50% B at 43 min, and 98% B from 44 to 48 min. The column was finally re-equilibrated in 2.5% B for 15 min. Full-scan MS spectra were acquired over a 300–1800 m/z range at a resolution of 120,000 (at 200 m/z), with an automatic gain control (AGC) target of 1×10^6 and a maximum injection time of 50 ms. The top 10 most intense precursor ions with an intensity exceeding 1.10^4 ions per second and charge states between 2 and 7 were automatically selected from each MS spectrum for higher-energy collisional dissociation (HCD) fragmentation at 30% normalized collision energy. MS/MS spectra were collected in the Orbitrap at a resolution of 15,000, with an AGC target of 1×10^5 and a maximum

injection time set to 22 ms. The complete system was fully controlled by Thermo Scientific™ Xcalibur™ software. Raw data collected were processed and converted with MSConvert into.mgf peak list format.

Data processing Search engine MASCOT 2.6.2 algorithm (Matrix Science) was used. The search was performed against the sequence of the light and heavy chains of the ADC. Spectra were searched with a mass tolerance of 10 ppm for MS and 0.05 Da for MS/MS data. The search was made without enzyme specified, in order to allow the identification of any non-specific cleavage peptide. Variable modifications were specified: oxidation of methionine residues, pyro-glutamylation of the N-termini, deamidation of asparagine, isomerization of aspartic acid residues, and drug-linker conjugation ($C_{52}FH_{56}N_9O_{13}$ and $C_{26}H_{32}O_8N_6$) on cysteine residues. Peptide identifications were validated with a minimal Mascot ion score of 30 using Proline Studio.

SEC-nMS analysis experiments

A Dionex UltiMate 3000 RSLC system (Thermo Scientific) was coupled to an Orbitrap Eclipse™ Tribrid™ (Thermo Fisher Scientific) mass spectrometer equipped with an EASY Max NG source with a heated electrospray ionization HESI probe. Fifteen micrograms and 12 µg were injected for intact and middle-up level analyses, respectively. The separation was carried out in isocratic mode with a 100 mM $AcONH_4$ mobile phase at pH 7 using an ACQUITY Protein BEH SEC 200 Å, 1.7 µm, 4.6 × 150 mm (Waters) SEC column. The flow rate was set to 250 µL/min for intact and middle-up analyses. The source parameters were set as follows: sheath gas flow rate to 25 a.u., auxiliary gas flow rate to 5 a.u., ion transfer capillary temperature to 275 °C, vaporizer temperature to 200 °C, and capillary voltage 3.8 kV. In-source fragmentation energy was set to 150 V and 50 V for the intact and middle-up analyses, respectively, and the RF Lens to 150%. Intact protein mode was activated, with a pressure of 20 mTorr in the ion routing multipole (high-pressure mode). Acquisitions were performed in the *m/z* range 500–8000 with a 3-ms scan and resolution of 15,000. The AGC target was set to 2×10^6, and the maximum injection time was 50 ms. Data were interpreted using BioPharma Finder v3.2 (Thermo Fisher Scientific, San Jose, CA, USA). The deconvolution mass tolerance was set to 10 ppm.

Middle-level LC-MS and LC-MS/MS analysis

Separation of the Fc/2, Fd, and LC subunits was performed with a BioResolve™ RP mAb polyphenyl column (450 Å pore size, 2.7 µm particle size, 2.1 × 150 mm, Waters) preheated at 60 °C, using a Dionex UltiMate 3000 RSLC system (Thermo Scientific). Mobile phase A consisted of 0.1% TFA in water, and mobile phase B was 0.1% TFA in ACN. For LC-MS and LC-MS/MS analyses, 3.5 µg and 5.5 µg of digested ADC were respectively loaded onto the column using 25% of mobile phase B at constant flow rate of 300 µL/min for 2 min. Digested ADC was eluted following a linear gradient: 25% at 2 min, 44% B at 40 min, and 75% B from 40.5 to 45.5 min. The column was finally re-equilibrated at 25% B for 15 min. The LC system was hyphenated to an Orbitrap Eclipse Tribrid mass spectrometer (Thermo Fisher Scientific, San Jose, CA) in intact protein mode. RF Lens was set to 60%, and auxiliary and sheath gases were set to 5 a.u. and 15 a.u., respectively. For all experiments, the spray voltage was set to 3.8 kV, the ion transfer tube temperature to 275 °C, the vaporizer to 200 °C, and the advanced peak determination was activated. MS spectra were recorded using a mass range of 500–4000 *m/z* and a resolving power of 120,000 (at 200 *m/z*) for denaturing middle-up analysis.

For middle-down analysis, three different fragmentation modes were used: CID, ETD, and EThcD; as well as the PTCR ion-ion reaction. MS^2 spectra were recorded using a mass range of 300–2000 *m/z*, a resolving power of 120,000 (at 200 *m/z*) and 2 micro scans per spectra were selected. Precursor ions were selected over each specific elution window with an isolation window of 3 *m/z* following subsequent fragmentation. For each subunit, the most intense, for CID, or the highest charge state, for ETD/EThcD, precursor ions were selected and submitted to fragmentation. The AGC was set to 1×10^6 and the maximum injection time to 200 ms for precursor ions. CID collision energy was set to 35%, with a CID activation time of 10 ms and an activation Q parameter of 0.25. For ETD fragmentation, the reaction time between precursor ions and the anionic fluoranthene reagent was 3 ms. To ensure proper precursor ions fragmentation, the anionic reagent target was set at 7×10^5 with a maximum reagent injection time of 200 ms. For EThcD fragmentation, the same parameters as those described for ETD were used, and a supplemental collision energy of 20% was used. PTCR was performed after ETD and EThcD fragmentation on either a wide isolation window of 1000 *m/z* (700–1700 *m/z*) or five isolation windows of 200 *m/z* between 700 and 1700 *m/z*. The PTCR reaction time was set to 20 ms for the wide isolation windows. For narrow windows, reaction times of either 5 ms (for 700–900 *m/z*, 1300–1500 *m/z*, and 1500–1700 *m/z* isolation windows) or 10 ms (for 900–1100 *m/z* and 1100–1300 *m/z* isolation windows) were used, depending on the ion population. The reagent target was set to 5×10^5 and the maximum reagent injection time to 200 ms. MS^3 spectra were recorded using a mass range of 500–4000 *m/z* and a resolving power of 120,000 (at 200 *m/z*), and 2 micro scans per spectra were selected.

Data analysis

MS/MS spectra were deconvoluted in FreeStyle 1.8 using the Xtract algorithm and deconvoluted masses were matched to the sequence using ProSight Lite v1.4. MS/MS spectra were averaged through the different subunit elution windows (0.5 min, 0.8 min, and 0.6 min for the Fc/2, Lc, and Fd subunits, respectively) and then deconvoluted using an S/N ratio of 7, a fit factor of 80%, and a remainder threshold of 25%. Deconvoluted masses were exported to.csv file and matched to the sequence with a 10-ppm tolerance. Different fragment ion series were considered depending on the fragmentation technique: *b*/*y* for CID, *c*/*z* for ETD, and *b*/*y* and *c*/*z* in the case of EThcD. Because of the DTT reduction performed during the sample preparation, all cysteines involved in intra-chain disulfide bridges were considered in their reduced form. In the case of the heavy chain and Fc/2 subunits, ions corresponding to the G0F glycoform were targeted, so G0F (+ 1444.5339 Da) at the Asp300 of the heavy chain (corresponding to Asp61 when Fc/2 is considered) was defined as a fixed modification to search the data. Drug conjugation (+ 1033.394 Da) on the cysteines involved in inter-chain disulfide bridges (Cys223, Cys229, and Cys232 on the Fd, Cys214 on the Lc) were set as fixed modifications.

For internal fragments analysis, ClipsMS [35] was used. Internal fragments were searched with an error tolerance of 2 ppm (10 ppm was kept for the terminal fragments) and the smallest internal fragment size of 5 amino acids. The following internal fragment ions were searched depending on the fragmentation method: *by* ions for CID, *cz* ions for ETD, and *by*, *cy*, *bz*, and *cz* ions for EThcD. Other parameters (modifications and terminal fragments tolerance) were set as mentioned above. For ions attributed to two different internal fragments, the assignment with the lower mass difference is kept and the other one is removed. If two (or more) fragments have exactly the same theoretical mass and mass difference with the assigned ion, then both identifications are kept.

Results and discussion

Intact and middle-level analysis of T-DXd for drug load distribution (DLD) determination and payload location assessment at the subunit level

The analysis of untreated T-DXd was first performed at the intact level with the use of the SEC-nMS coupling to confirm the drug load distribution (DLD) and the avDAR values of the ADC. Intact T-DXd analysis results in the identification of homogeneous T-DXd (and its glycoforms) bearing 8 conjugated drugs (avDAR of 8.0) in agreement with previously reported data [13] (Supplementary Figure S1).

We next performed classical RPLC-MS to separate and characterize the subunits of T-DXd obtained either after reduction (heavy (Hc) and light chains (Lc)) or upon IdeS digestion followed by DTT reduction (Lc, Fd, Fc/2 subunits, Supplementary Figure S2). Reduced T-DXd analysis reveals two main species eluting at 23.6 min and 30.5 min (Supplementary Figure S2.A). The first one corresponds to the Lc carrying one drug (24,476.9 ± 0.2 Da, Supplementary Figure S2.B and Supplementary Table S1) and the second one to the Hc with three conjugated drugs (53,703.6 ± 0.4 Da for the main glycoform G0F, Supplementary Figure S2.C and Supplementary Table S1). Both peaks exhibit additional populations at slightly lower retention times corresponding to the binding of partial payload scaffolds (− 475 Da) [13]. The analysis of IdeS digested and reduced T-DXd showed three main peaks (Supplementary Figure S2.D), corresponding to the Fc/2 (23,235.9 ± 0.3 Da for the main glycoform G0F, Supplementary Figure S2.E), Lc with one drug (24,476.9 ± 0.2 Da, Supplementary Figure S2.F) and Fd bearing three drugs (28,485.5 ± 0.2 Da, Supplementary Figure S2.G) subunits, respectively. In line with previous results for reduced T-DXd, minor chromatographic peaks resulting from Lc and Fd bearing partial drug(s) (− 475 Da) are observed prior to the major chromatographic peaks of these subunits, but no drug-free species were detected. In addition, no signal corresponding to free Lc or Hc was detected. All these results regarding the absence of drug-free and/or partially conjugated species underline the high efficiency of the conjugation process for T-DXd. Middle-up level RPLC-MS analysis corroborates the location of 3 drugs on the Hc/Fd domain and one on the Lc domain, correlating with a homogeneous avDAR 8.0 calculated previously.

Middle-down mass spectrometry (MD-MS) analysis for sequence characterization and precise drug location

We next performed MD-MS analyses of T-DXd at the subunit level. The precursor ions selected for MS/MS fragmentation are displayed in Supplementary Figure S2 and detailed in the "Materials and methods" for each considered subunit. The most abundant charge state was selected for CID, while highly charged precursors were preferred for electron-based fragmentations (ETD and EThcD). Conversely to classical bottom-up strategies where sequence coverages are optimized, usually leading to accurate identification of drug location, we decided here to first address the position of the payloads by monitoring the sequence coverage as a function of payloads bound to different cysteine residues. Once the "most probable" conjugation site was determined, the MS/MS data obtained from each replicate of each fragmentation technique were combined to increase the overall sequence coverage of the subunits (9 runs combined).

For reduced T-DXd, Lc+1DXd or Hc+3DXd species were selected for further CID, ETD, and EThcD fragmentation. In this context, the MS/MS spectra of the Lc were matched with 5 different positional isomer sequences (5 Cys residues in the Lc sequence), while those of the Hc were compared with the sequence of 165 different isomers (combinations of 3 conjugated Cys residues out of 11 Cys, Supplementary Figure S3). From Lc MS/MS data interpretation, it can be concluded that the conjugation site is located on the C-terminal part (Cys194 or Cys214, Fig. 1A–C), as higher sequence coverages (14%/38%/42% for CID/ETD/EThcD for Cys194-DXd, and 14%/39%/42% for CID/ETD/EThcD for Cys214-DXd) were achieved when considering DXd bound to one of those Cys residues. However, the z_{12}

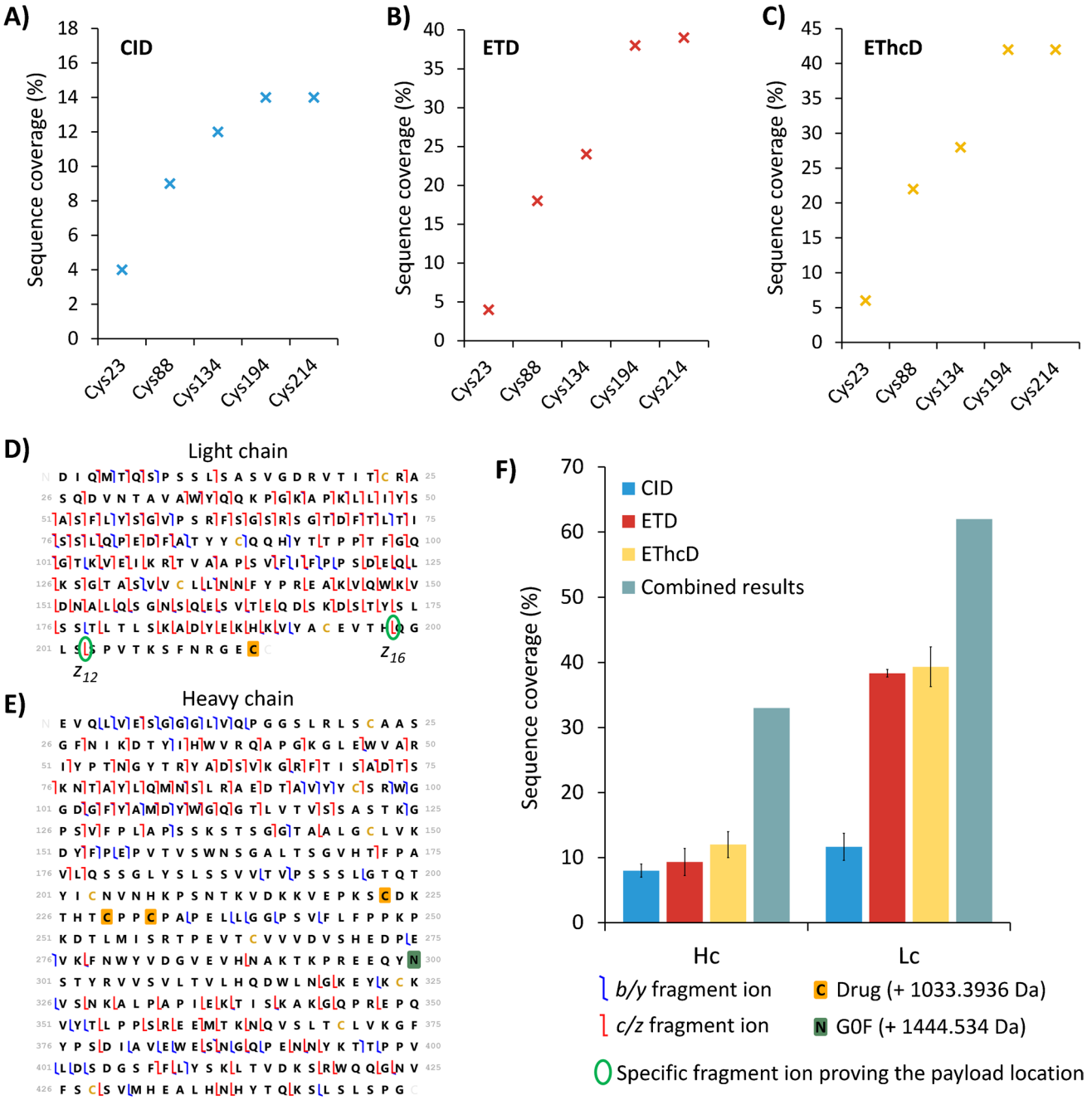

Fig. 1 Fragmentation results for the T-DXd heavy (Hc) and light chains (Lc). CID (**A**), ETD (**B**), and EThcD (**C**) light chain sequence coverage depending on the conjugated cysteine position. (**D**) Light chain fragmentation map of the combined results from all replicates. (**E**) Heavy chain fragmentation map of the combined results from all replicates. (**F**) Hc and Lc average sequence coverage obtained by CID (blue), ETD (red), and EThcD (yellow) for three injection replicates, and the combined results from all runs (green)

fragment ion obtained in 3 over 3 ETD and EThcD replicates and the z_{16} obtained in 3 over 3 ETD replicates both allow determining that the payload is precisely located on Cys214 residue (Fig. 1D). Data interpretation is even more challenging for Hc (Fig. 1E) as the sequence coverage obtained is similar (8–11%) when considering the theoretical positions (i.e., Cys223, Cys229, and Cys232) of the payloads (Supplementary Figure S4), regardless of the activation technique used to induce the fragmentation. The fragmentation map of the combined results (9 runs) for the Hc clearly points out the absence of fragmentation in the middle of the Hc sequence, which impairs the reliable location of the conjugation sites in this chain (Fig. 1E). As expected, electron-based fragmentations (ETD/EThcD) afforded the most complete sequence coverage for both chains (39% for Lc and 12% for Hc), as already reported on other systems [28]. Finally, sequence coverage upon combining CID, ETD, and EThcD fragmentation replicates raised to 62% for the Lc and 33% for the Hc (Fig. 1F), which is still relatively low. Our results are in line with sequence coverages previously reported [48, 49], which can be explained by the difficulty of providing a complete sequence coverage characterization when fragmenting proteins larger than 30 kDa [50]. In the particular case of the Hc, this limited fragmentation hampers the precise location of the conjugation sites.

In order to increase the sequence coverage and locate more precisely the conjugation sites, T-DXd was IdeS digested and reduced to release the three ~ 25 kDa subunits (Fc/2, Lc, and Fd) and subsequently fragmented using the aforementioned activation modes (Supplementary Figure S5). Similar to results obtained on Lc generated after DTT treatment, MD-MS results obtained after IdeS digestion allow to conclude that DXd is located on the Cys214 of Lc (Fig. 2A), as the two same diagnostic fragments specific of the drug conjugation on Cys214 were identified (z_{12} and z_{16}, Supplementary Figure S6.A) upon ETD/EThcD fragmentation (in 3/3 and 2/3 replicates, respectively). As IdeS digestion efficiently downsized the Hc chain, we next analyzed the results from the 35 possible Fd isomers (3 conjugated Cys residues out of 7 Cys residues in the Fd, see Supplementary Figure S3). It came out that proteoforms including conjugated C-terminal Cys (i.e., Cys203, Cys223, Cys229, and Cys 232) led to the highest sequence coverage (Fig. 2B), suggesting possible DXd location on abovementioned Cys. Nevertheless, 7 fragments (all from ETD/EThcD and assigned in at least 2/3 replicates for each fragmentation technique) corroborated the presence of the payloads on the 3 C-terminal Cys residues involved in inter-chain disulfide bridges of the mAb counterpart (Supplementary Figure S6.B). Here, we observed fragment ions confirming the drug location for both Lc (Cys214) and Fd subunits (Cys223, Cys229, and Cys232). Moreover, after manual validation, it was confirmed that those ions exhibited resolved isotope profiles with no interfering signals and with a significant S/N ratio (> 150), thus increasing the confidence in their identification (Supplementary Figure S6.C and S7).

The conjugation sites inferred from MD-MS strategies were corroborated with bottom-up analysis (Supplementary Figure S8), with no detection of additional conjugation sites by the latter technique, highlighting the complementarity between both strategies. However, peptide mapping results still evidence the difficulties of this approach to decipher the drug conjugation of an ADC, as only a few fragments contain the whole payload scaffold and the location of the conjugation site is performed by detecting payload-bound peptide ions, with the detection of a specific signature fragment ion coming from the fragmentation of the cargo molecule (Supplementary Figure S6).

Best sequence coverages achieved for T-DXd subunits for each individual fragmentation technique ranged between 29 and 61% for Fc/2, 15–48% for Lc, and 19–37% for Fd, with best results originating from EThcD fragmentation (61%, 48%, and 37% with EThcD for the Fc/2, Lc, and Fd parts, respectively). Between 40 and 55% of all the identified terminal ions were observed in all the replicates of the same fragmentation technique, and the individual p-scores associated to the different subunits with the precise conjugation site were lower than 10^{-10} for CID, 10^{-20} for EThcD, and 10^{-37} for ETD. Interestingly, combining replicates from all fragmentation modes resulted in a high sequence coverage for the Fc/2, Lc, and Fd subunits with 87%, 76%, and 72%, respectively (Fig. 2C) covering not only both termini of the sequences but also the internal regions as expected when fragmenting 25-kDa subunits.

Altogether, MD-MS investigations of T-DXd subunits confirm the payloads conjugation on the Cys214 for the Lc (with z_{12} and/or z_{16} specific diagnostic ions), while DXd binding could only be restricted to the C-terminal area of the Fd subunit (Cys223, Cys229, or Cys232) with the detection of 7 specific fragment ions. As expected, MD-MS results in terms of sequence coverage were better with EThcD and after IdeS digestion, in which smaller subunits (~ 25–30 kDa) were more adapted to MD-MS analysis.

Contribution of internal fragments in the context of T-DXd subunits sequence characterization

In classical TD/MD-MS experiments, only N- and C- terminal fragments (originating from one single cleavage site in the protein backbone) are matched to determine the sequence coverage. However, protein backbone can undergo subsequent residue cleavages leading to the formation of internal fragments that are not containing neither the N- nor the C-terminus of the protein. ClipsMS [35] was used to tackle internal fragments generated in our MD-MS workflow. Terminal fragments were assigned first using a 10-ppm

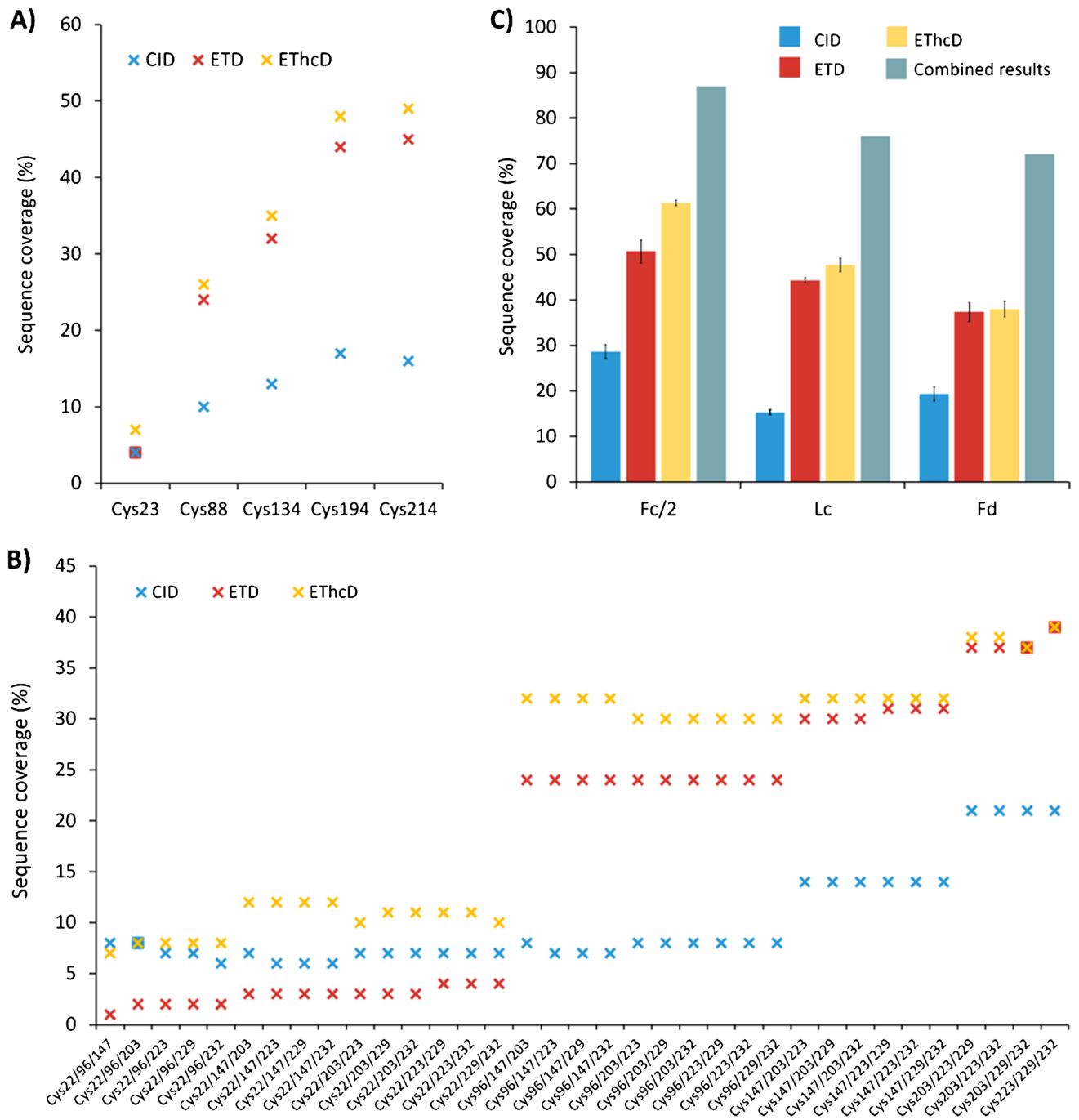

Fig. 2 Fragmentation results for the T-DXd Fc/2, Fd, and Lc subunits. Lc (**A**) and Fd (**B**) sequence coverage depending on the conjugated cysteine positions for CID (blue), ETD (red), and EThcD (yellow). (**C**) Fc/2, Lc, and Fd average sequence coverage obtained by CID (blue), ETD (red), and EThcD (yellow) for three injection replicates, and the combined results of all runs (green)

tolerance (same as with ProSight Lite). Then, internal fragments were assigned using a 2-ppm tolerance to limit the risk of false assignment.

Initially, the contribution of internal fragments was evaluated to determine the position of the payload of the subunits. It was found that those fragments are not particularly adapted to decipher the position for several reasons. Payloads are mainly located in the C-terminal region of the Lc and Fd subunits, and hence, very low amounts of internal fragments will contain the payload moiety. Conversely to terminal fragments, the sequence coverage variation obtained upon consideration of internal fragment ions is less sensitive to the position of the payload. For instance, the sequence coverage of the Lc subunit upon ETD fragmentation increases from 4

to 45% when the conjugation site is assumed either at Cys23 or Cys214, respectively, clearly pinpointing that the conjugation site is located in the latter residue. However, upon internal fragment matching, the sequence coverage variation between these two conjugated positions is more attenuated (from 51 to 67%), leading to a more ambiguous result.

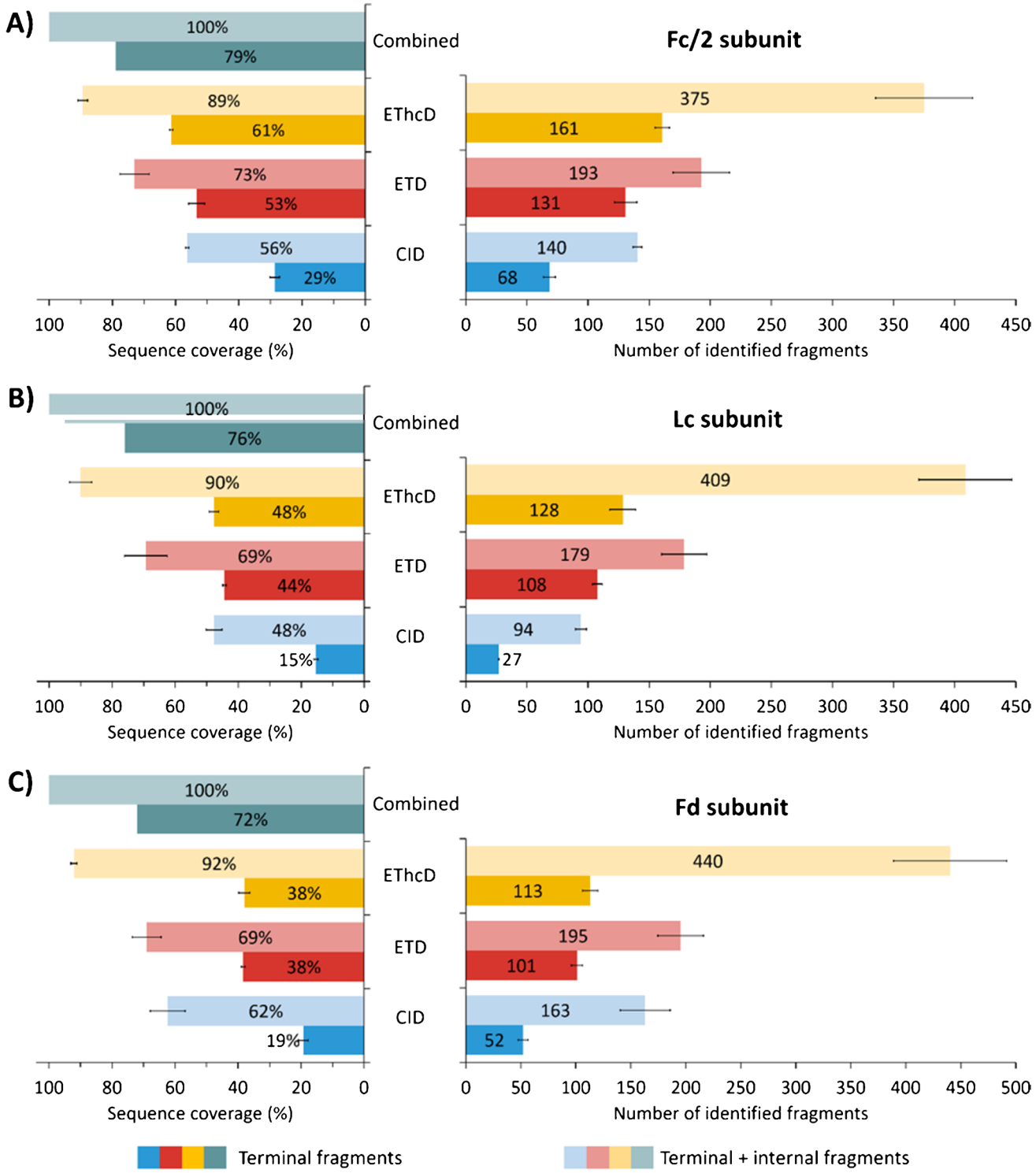

Fig. 3 Average sequence coverage and number of fragments identified for T-DXd Fc/2, Fd, and Lc subunits using internal fragments. Average sequence coverage (left) and number of identified fragments (right) considering the terminal fragments only (dark colors) and terminal + internal fragments (light colors) for CID (blue), ETD (red), and EThcD (yellow) of Fc/2 (**A**), LC (**B**), and Fd (**C**) subunits. The results of the individual fragmentation techniques were run in triplicate and the combined results are depicted in green

Finally, it was observed that internal fragment consideration entails an increased probability of ion mismatching [45]. For example, the search for internal fragments after ETD by positioning the drug on the Cys23 residue of the Lc leads to the detection of more than 20 internal fragments containing the drug. More precisely, one identified internal fragment exhibits a clear isotopic profile with a very precise mass measurement that could correspond with the 21–52 internal fragment bearing the payload (4523.22 Da, Supplementary Figure S9). Nevertheless, the Cys23 conjugation site was excluded from our previous MD-MS results based on terminal fragment identification because of the low sequence coverage assigned to this position. The golden-standard bottom-up method did not provide any peptide containing the drug at position 23, clearly suggesting that all those ions could not correspond to the fragmentation of a bunch of the Lc backbone with conjugated Cys23. For all these reasons, the characterization of the conjugation sites relied on the identification of terminal fragments, while internal fragment ions were used with the main purpose of boosting the sequence coverage of the different subunits.

The proportion of internal fragments identified differs with the fragmentation method. Depending on the subunit, the average number of internal fragments identified varies between 72 and 111 for CID, 62 and 94 for ETD, and 214 and 327 for EThcD. As expected, EThcD provides the higher number of internal fragments resulting from the addition of a collisional-activation step of ions that have been previously activated/dissociated upon electron transfer. In the end, a total number of fragments (terminal and internal) around 130, 200, and 400 for CID, ETD, and EThcD, respectively, were detected (Fig. 3A–C, right). Consequently, the sequence coverage drastically increased when including internal fragments to reach 50 to 60% with CID (15–30% considering terminal fragments only), 70% with ETD (38–53% considering terminal fragments only), and 90% for EThcD (38–61% considering terminal fragments only) (Fig. 3A–C, left). Manual validation of the internal fragments identified can help to ascertain the confidence in the match, and it was found that internal fragments were relatively well resolved (Supplementary Figure S10). Combining the sequence coverage from replicates of all the fragmentation techniques (i.e., CID, ETD, and EThcD) resulted in 100% subunit sequence confirmation (Fig. 3). Concomitantly, the relative proportion of assigned fragment ions increased by 1.6 to 3 times when using internal fragment ion searching. However, poor reproducibility between different replicates was observed regarding the internal fragment identification since only around 20% of the total number of the internal fragments were detected in at least 2 over 3 replicates (and less than 5% in 3 over 3 replicates). These results clearly show that considering internal fragment ion search during MD-MS workflows allows taking full advantage of all the information contained in the MS/MS spectra, highlighting the contribution of internal fragments to increase the sequence coverage although care must be taken to reduce the number of false or ambiguous assignments.

Strengthening drug location using proton transfer charge reduction (PTCR)

While the attribution of internal fragments allows obtaining the complete sequence coverage by exploiting the huge amount of information available from MS^2 spectra, the risk of false positives and the position of the payloads on the C-termini of the sequences make its contribution limited to the identification of the conjugation sites. With this in mind, PTCR was combined with the most efficient fragmentation, i.e., ETD and EThcD, to declutter MS^2 spectra and confirm drug location. To do so, two different PTCR methods were used: (i) the "wide window" (1000 *m/z* isolation window) method and (ii) the "narrow window" (5 × 200 *m/z* isolation window) mode (Supplementary Figure S11). As highlighted in Fig. 4A and B, the combination of PTCR results from all the windows leads to an average rise of the sequence coverage by 10–13% after ETD fragmentation and by 2–7% after EThcD fragmentation, respectively. The practical effect of this ion/ion reaction is further illustrated in Supplementary Figure S8. After ETD fragmentation, a complex MS^2 spectrum is generated, with a very large number of fragments distributed only over a small *m/z* range (700–1700 *m/z*, Supplementary Figure S8.A). Using PTCR for 10 ms on the 1100–1300 *m/z* window drastically reduced the spectral congestion of this zone of the MS^2 spectrum, decreasing the signal interference in the lower *m/z*, where the major part of the fragment ions of interest are observed. For instance, overlapping signals and interferences are observed in the ETD MS^2 spectrum of the diagnostic fragment ion z_{12} (2341.00 Da), which allows the precise location of the DXd on the Lc (Supplementary Figure S12.A). Thanks to the addition of PTCR, the same ion could be assigned with a resolved isotope profile and a low interfering signal, leading to a more reliable identification of the fragment (Supplementary Figure S8.B). The PTCR MS^2 spectra decluttering capabilities not only afforded more confident identification of diagnostic ions detected without PTCR but, more interestingly, allowed

Fig. 4 PTCR fragmentation results for the T-DXd Fc/2, Lc, and Fd subunits. (**A**) Fc/2, Lc, and Fd average sequence coverage obtained by ETD only (light red) and ETD + PTCR (dark red) for the three injection replicates. (**B**) Fc/2, Lc, and Fd average sequence coverage obtained by EThcD only (light yellow) and EThcD + PTCR (dark yellow) for the three injection replicates. Fragmentation maps combining ETD/EThcD MS^2 and PTCR MS^3 results of the Lc (**C**) and Fd (**D**) subunits. Fragments found uniquely thanks to PTCR are circled in black and those confirming the position of the drugs are circled in green

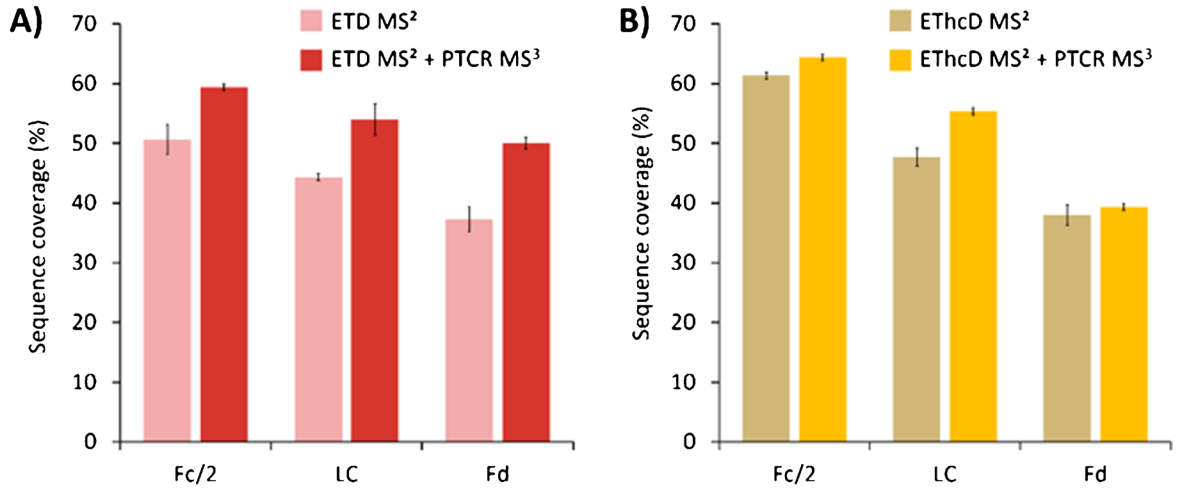

C)

Lc subunit

N D I Q M T Q S P S S L S A S V G D R V T I T C R A 25
26 S Q D V N T A V A W Y Q Q K P G K A P K L L I Y S 50
51 A S F L Y S G V P S R F S G S R S G T D F T L T I 75
76 S S L Q P E D F A T Y Y C Q Q H Y T T P P T F G Q 100
101 G T K V E I K R T V A A P S V F I F P P S D E Q L 125
126 K S G T A S V V C L L N N F Y P R E A K V Q W K V 150
151 D N A L Q S G N S Q E S V T E Q D S K D S T Y S L 175
176 S S T L T L S K A D Y E K H K V Y A C E V T H Q G 200
201 L S S P V T K S F N R G E C 225

D)

Fd subunit

N E V Q L V E S G G G L V Q P G G S L R L S C A A S 25
26 G F N I K D T Y I H W V R Q A P G K G L E W V A R 50
51 I Y P T N G Y T R Y A D S V K G R F T I S A D T S 75
76 K N T A Y L Q M N S L R A E D T A V Y Y C S R W G 100
101 G D G F Y A M D Y W G Q G T L V T V S S A S T K G 125
126 P S V F P L A P S S K S T S G G T A A L G C L V K 150
151 D Y F P E P V T V S W N S G A L T S G V H T F P A 175
176 V L Q S S G L Y S L S S V V T V P S S S L G T Q T 200
201 Y I C N V N H K P S N T K V D K K V E P K S C D K 225
226 T H T C P P C P A P E L L G 240

O Additional fragment ions found using PTCR

O Additional fragment ions found using PTCR and confirming the presence of the drugs

identification of additional specific diagnostic fragment ions on the different subunits. Upon addition of PTCR, a total of 5 fragment ions specific of the Cys214 conjugation on the Lc (2 fragments found with ETD/EThcD and 3 additional found after PTCR implementation, z_{13}, y_{19}, and y_{20}, all in at least 2/3 replicates, Fig. 4C) and 11 signature fragments specific of the conjugation of the Fd subunit on the Cys223, Cys229, and Cys232 residues (7 fragments found with ETD/EThcD and 4 additional fragments detected after PTCR implementation, z_{26}, z_{27}, z_{30}, and z_{32}, all identified in at least 2/3 replicates, Fig. 4D) were finally detected. For instance, the fragment z_{26} that was not observed at any charge states using ETD only is assigned after the use of PTCR for 10 ms on the 1300–1500 m/z mass range, as the 4 + charge state has been detected and presents a well-resolved isotopic profile (Supplementary Figure S13). These results highlight that PTCR contributes to the improvement of the overall sequence coverage to a lesser extent compared to internal fragment ion search but enhances the number and confidence of identified diagnostic fragment ions of the conjugation site, providing additional experimental evidence to locate the sequence modifications of interest.

Conclusions

In this study, several MS-based techniques have been combined to characterize a homogeneous DAR8 ADC, T-DXd.

The different subunits bearing the cargo molecules were subjected to fragmentation to elucidate the conjugation sites. Results evidenced that the precise location of the three payloads from the fragmentation of the entire Hc was still challenging due to the lack of fragmentation in the mid-region of the backbone. In this case, the fragmentation of the Fd subunit was more informative, providing a more comprehensive sequence coverage along with a significant number of signature fragment ions characteristic of the three conjugated cysteine residues.

PTCR reaction and tailored TD/MD-MS software were used to maximize the number of identified fragment ions. The identification of internal fragments with the use of ClipsMS helped to confirm the whole sequence of the ADC, giving rise to the characterization of the full sequence of each subunit. Although very informative to improve the overall sequence coverage, special care should be taken when considering internal fragment ions since the probabilities for false positive ion assignment increase, providing ambiguous results about the precise location of the cytotoxic payload in the sequence of the ADC.

PTCR emerged as an elegant alternative to explore more deeply the fragmentation spectra information. This technique led to an overall sequence coverage increase between 2 and 13% for each ADC subunit. In spite of the moderate sequence coverage contribution of PTCR, the enhanced separation of charge-reduced fragment ions allowed for increasing the confidence of the location of the conjugation sites by increasing the number of diagnostic ions by 1.5- to 2.5-fold. According to these results, the combination of a single activation technique (i.e., ETD or EThcD) with PTCR reaction can be an appealing alternative to the combination of multiple activation techniques (CID, HCD, ETD, EThcD, UVPD) that will afford additional information to characterize the sequence modification of interest.

Altogether, these results highlight the potential of combining different MS-based approaches, with particular interest in cutting-edge MD-MS strategies, in the characterization of approved therapeutic proteins to evaluate the homogeneity of the bioconjugation with limited sample preparation. More particularly, the contribution of MD-MS workflows in the conjugation site characterization of ADCs has been clearly shown in comparison with classical bottom-up approaches, facilitating the identification of fragment ions containing the whole payload, which is a significant limitation when ADCs are characterized at the peptide level. Hopefully, the continuous development of tailored software and the implementation of novel strategies in last-generation MS platforms will foster the use of intact or partially digested protein fragmentation in different R&D laboratories, especially (but not exclusively) those dedicated to the analysis of therapeutic proteins.

Supplementary Information The online version contains supplementary material available at https://doi.org/10.1007/s00216-023-05059-x.

Acknowledgements The authors acknowledge Alexandre Detappe (ICANS, Strasbourg, France) for providing the samples.

Author contribution CB: methodology, investigation, formal analysis, data curation, writing—original draft preparation, reviewing and editing

CC: writing—reviewing and editing

ED: investigation, writing—reviewing and editing

HD: investigation, formal analysis, data curation, writing—reviewing and editing

OHA: conceptualization, supervision, writing—original draft preparation, reviewing, and editing

SC: resources, writing—reviewing and editing

Funding This work was supported by the CNRS, and the "Agence Nationale de la Recherche" via the French Proteomic Infrastructure (ProFI FR2048; ANR-10-INBS-08-03), the ConformAbs project (ANR-21-CE29-0009-01), by the Région Grand-Est (Fonds Régional de la Coopération pour la Recherche, HRMS-INFECT project) and by the French Ministry of Higher Education and Research for the PhD fellowship of C.B.

Declarations

Conflict of interest The authors declare no competing interests.

References

1. Kaplon H, Chenoweth A, Crescioli S, Reichert JM. Antibodies to watch in 2022. mAbs. 2022;14(1):2014296.
2. Kaplon H, Crescioli S, Chenoweth A, Visweswaraiah J, Reichert JM. Antibodies to watch in 2023. mAbs. 2023;15(1):2153410.
3. Fu Z, Li S, Han S, Shi C, Zhang Y. Antibody drug conjugate: the "biological missile" for targeted cancer therapy. Signal Transduct Target Ther. 2022;7(1):93.
4. Joubert N, Beck A, Dumontet C, Denevault-Sabourin C. Antibody-drug conjugates: the last decade. Pharmaceuticals (Basel). 2020;13(9):245.
5. Nadkarni DV. Conjugations to endogenous cysteine residues. Methods Mol Biol (Clifton, NJ). 2020;2078:37–49.
6. Haque M, Forte N, Baker JR. Site-selective lysine conjugation methods and applications towards antibody-drug conjugates. Chem Commun (Camb). 2021;57(82):10689–702.
7. Sadiki A, Vaidya SR, Abdollahi M, Bhardwaj G, Dolan ME, Turna H, et al. Site-specific conjugation of native antibody. Antib Ther. 2020;3(4):271–84.
8. Adhikari P, Zacharias N, Ohri R, Sadowsky J. Site-specific conjugation to Cys-engineered THIOMAB™ antibodies. Methods Mol Biol (Clifton, NJ). 2020;2078:51–69.
9. Hallam TJ, Wold E, Wahl A, Smider VV. Antibody conjugates with unnatural amino acids. Mol Pharm. 2015;12(6):1848–62.
10. Diamantis N, Banerji U. Antibody-drug conjugates–an emerging class of cancer treatment. Br J Cancer. 2016;114(4):362–7.
11. Xu Y, Wang D, Mason B, Rossomando T, Li N, Liu D, et al. Structure, heterogeneity and developability assessment of therapeutic antibodies. mAbs. 2019;11(2):239–64.
12. Beck A, D'Atri V, Ehkirch A, Fekete S, Hernandez-Alba O, Gahoual R, et al. Cutting-edge multi-level analytical and structural characterization of antibody-drug conjugates: present and future. Expert Rev Proteomics. 2019;16(4):337–62.
13. Deslignière E, Diemer H, Erb S, Coliat P, Pivot X, Detappe A, et al. A combination of native LC-MS approaches for the comprehensive characterization of the antibody-drug conjugate trastuzumab deruxtecan. Front Biosci (Landmark Ed). 2022;27(10):290.
14. van Schaick G, Haselberg R, Somsen GW, Wuhrer M, Domínguez-Vega E. Studying protein structure and function by native separation-mass spectrometry. Nat Rev Chem. 2022;6(3):215–31.
15. Donnelly DP, Rawlins CM, DeHart CJ, Fornelli L, Schachner LF, Lin Z, et al. Best practices and benchmarks for intact protein analysis for top-down mass spectrometry. Nat Methods. 2019;16(7):587–94.
16. Brodbelt JS. Deciphering combinatorial post-translational modifications by top-down mass spectrometry. Curr Opin Chem Biol. 2022;70: 102180.
17. Chapman EA, Aballo TJ, Melby JA, Zhou T, Price SJ, Rossler KJ, et al. Defining the sarcomeric proteoform landscape in ischemic cardiomyopathy by top-down proteomics. J Proteome Res. 2023;22(3):931–41.
18. Jeanne Dit Fouque K, Miller SA, Pham K, Bhanu NV, Cintron-Diaz YL, Leyva D, et al. Top-"double-down" mass spectrometry of histone H4 proteoforms: tandem ultraviolet-photon and mobility/mass-selected electron capture dissociations. Anal Chem. 2022;94(44):15377–85.
19. Lodge JM, Schauer KL, Brademan DR, Riley NM, Shishkova E, Westphall MS, et al. Top-down characterization of an intact monoclonal antibody using activated ion electron transfer dissociation. Anal Chem. 2020;92(15):10246–51.
20. Jin Y, Lin Z, Xu Q, Fu C, Zhang Z, Zhang Q, et al. Comprehensive characterization of monoclonal antibody by Fourier transform ion cyclotron resonance mass spectrometry. mAbs. 2019;11(1):106–15.
21. He L, Anderson LC, Barnidge DR, Murray DL, Hendrickson CL, Marshall AG. Analysis of monoclonal antibodies in human serum as a model for clinical monoclonal gammopathy by use of 21 Tesla FT-ICR top-down and middle-down MS/MS. J Am Soc Mass Spectrom. 2017;28(5):827–38.
22. van der Burgt YEM, Kilgour DPA, Tsybin YO, Srzentić K, Fornelli L, Beck A, et al. Structural analysis of monoclonal antibodies by ultrahigh resolution MALDI in-source decay FT-ICR mass spectrometry. Anal Chem. 2019;91(3):2079–85.
23. Shaw JB, Liu W, Vasil Ev YV, Bracken CC, Malhan N, Guthals A, et al. Direct determination of antibody chain pairing by top-down and middle-down mass spectrometry using electron capture dissociation and ultraviolet photodissociation. Anal Chem. 2020;92(1):766–73.
24. Kellie JF, Schneck NA, Causon JC, Baba T, Mehl JT, Pohl KI. Top-down characterization and intact mass quantitation of a monoclonal antibody drug from serum by use of a quadrupole TOF MS system equipped with electron-activated dissociation. J Am Soc Mass Spectrom. 2023;34(1):17–26.
25. Watts E, Williams JD, Miesbauer LJ, Bruncko M, Brodbelt JS. Comprehensive middle-down mass spectrometry characterization of an antibody-drug conjugate by combined ion activation methods. Anal Chem. 2020;92(14):9790–8.
26. Larson EJ, Roberts DS, Melby JA, Buck KM, Zhu Y, Zhou S, et al. High-throughput multi-attribute analysis of antibody-drug conjugates enabled by trapped ion mobility spectrometry and top-down mass spectrometry. Anal Chem. 2021;93(29):10013–21.
27. Chen B, Lin Z, Zhu Y, Jin Y, Larson E, Xu Q, et al. Middle-down multi-attribute analysis of antibody-drug conjugates with electron transfer dissociation. Anal Chem. 2019;91(18):11661–9.
28. Hernandez-Alba O, Houel S, Hessmann S, Erb S, Rabuka D, Huguet R, et al. A case study to identify the drug conjugation site of a site-specific antibody-drug-conjugate using middle-down mass spectrometry. J Am Soc Mass Spectrom. 2019;30(11):2419–29.
29. Sang H, Lu G, Liu Y, Hu Q, Xing W, Cui D, et al. Conjugation site analysis of antibody-drug-conjugates (ADCs) by signature ion fingerprinting and normalized area quantitation approach using nano-liquid chromatography coupled to high resolution mass spectrometry. Anal Chim Acta. 2017;955:67–78.
30. Bashyal A, Dunham SD, Brodbelt JS. Characterization of unbranched ubiquitin tetramers by combining ultraviolet photodissociation with proton transfer charge reduction reactions. Anal Chem. 2023;95(37):14001–8.
31. Walker JN, Lam R, Brodbelt JS. Enhanced characterization of histones using 193 nm ultraviolet photodissociation and proton transfer charge reduction. Anal Chem. 2023;95(14):5985–93.
32. Huguet R, Mullen C, Srzentić K, Greer JB, Fellers RT, Zabrouskov V, et al. Proton transfer charge reduction enables high-throughput top-down analysis of large proteoforms. Anal Chem. 2019;91(24):15732–9.
33. Dunham SD, Wei B, Lantz C, Loo JA, Brodbelt JS. Impact of internal fragments on top-down analysis of intact proteins by 193 nm UVPD. J Proteome Res. 2023;22(1):170–81.
34. Kline JT, Mullen C, Durbin KR, Oates RN, Huguet R, Syka JEP, et al. Sequential ion-ion reactions for enhanced gas-phase sequencing of large intact proteins in a tribrid Orbitrap mass spectrometer. J Am Soc Mass Spectrom. 2021;32(9):2334–45.
35. Lantz C, Zenaidee MA, Wei B, Hemminger Z, Ogorzalek Loo RR, Loo JA. ClipsMS: an algorithm for analyzing internal fragments resulting from top-down mass spectrometry. J Proteome Res. 2021;20(4):1928–35.
36. Schmitt ND, Berger JM, Conway JB, Agar JN. Increasing top-down mass spectrometry sequence coverage by an order of magnitude through optimized internal fragment generation and assignment. Anal Chem. 2021;93(16):6355–62.

37. Stephenson JL Jr, McLuckey SA. Simplification of product ion spectra derived from multiply charged parent ions via ion/ion chemistry. Anal Chem. 1998;70(17):3533–44.
38. Rolfs Z, Smith LM. Internal fragment ions disambiguate and increase identifications in top-down proteomics. J Proteome Res. 2021;20(12):5412–8.
39. Wei B, Lantz C, Liu W, Viner R, Ogorzalek Loo RR, Campuzano IDG, et al. Added value of internal fragments for top-down mass spectrometry of intact monoclonal antibodies and antibody-drug conjugates. Anal Chem. 2023;95(24):9347–56.
40. Lyon YA, Riggs D, Fornelli L, Compton PD, Julian RR. The ups and downs of repeated cleavage and internal fragment production in top-down proteomics. J Am Soc Mass Spectrom. 2018;29(1):150–7.
41. Zenaidee MA, Lantz C, Perkins T, Jung W, Loo RRO, Loo JA. Internal fragments generated by electron ionization dissociation enhance protein top-down mass spectrometry. J Am Soc Mass Spectrom. 2020;31(9):1896–902.
42. Zenaidee MA, Wei B, Lantz C, Wu HT, Lambeth TR, Diedrich JK, et al. Internal fragments generated from different top-down mass spectrometry fragmentation methods extend protein sequence coverage. J Am Soc Mass Spectrom. 2021;32(7):1752–8.
43. Wei B, Zenaidee MA, Lantz C, Ogorzalek Loo RR, Loo JA. Towards understanding the formation of internal fragments generated by collisionally activated dissociation for top-down mass spectrometry. Anal Chim Acta. 2022;1194: 339400.
44. Wei B, Zenaidee MA, Lantz C, Williams BJ, Totten S, Ogorzalek Loo RR, et al. Top-down mass spectrometry and assigning internal fragments for determining disulfide bond positions in proteins. Analyst. 2022;148(1):26–37.
45. Dunham SD, Wei B, Lantz C, Loo JA, Brodbelt JS. Impact of internal fragments on top-down analysis of intact proteins by 193 nm UVPD. J Proteome Res. 2022;22(1):170–81.
46. Nakada T, Masuda T, Naito H, Yoshida M, Ashida S, Morita K, et al. Novel antibody drug conjugates containing exatecan derivative-based cytotoxic payloads. Bioorg Med Chem Lett. 2016;26(6):1542–5.
47. Ogitani Y, Aida T, Hagihara K, Yamaguchi J, Ishii C, Harada N, et al. DS-8201a, A novel HER2-targeting ADC with a novel DNA topoisomerase I inhibitor, demonstrates a promising antitumor efficacy with differentiation from T-DM1. Clin Cancer Res. 2016;22(20):5097–108.
48. Dhenin J, Dupré M, Druart K, Krick A, Mauriac C, Chamot-Rooke J. A multiparameter optimization in middle-down analysis of monoclonal antibodies by LC-MS/MS. J Mass Spectrom JMS. 2023;58(3): e4909.
49. Melani RD, Srzentić K, Gerbasi VR, McGee JP, Huguet R, Fornelli L, et al. Direct measurement of light and heavy antibody chains using ion mobility and middle-down mass spectrometry. mAbs. 2019;11(8):1351–7.
50. Fornelli L, Parra J, Hartmer R, Stoermer C, Lubeck M, Tsybin YO. Top-down analysis of 30–80 kDa proteins by electron transfer dissociation time-of-flight mass spectrometry. Anal Bioanal Chem. 2013;405(26):8505–14.